Science Signaling
AAAS

www.sciencesignaling.org/cgi/content/full/6/289/ra70/DC1

Supplementary Materials for

Conserved Regulators of Nucleolar Size Revealed by Global Phenotypic Analyses

Ralph A. Neumüller, Thomas Gross, Anastasia A. Samsonova, Arunachalam Vinayagam, Michael Buckner, Karen Founk, Yanhui Hu, Sara Sharifpoor, Adam P. Rosebrock, Brenda Andrews, Fred Winston,* Norbert Perrimon*

*Corresponding author. E-mail: perrimon@receptor.med.harvard.edu (N.P.); winston@genetics.med.harvard.edu (F.W.)

Published 20 August 2013, *Sci. Signal.* **6**, ra70 (2013)
DOI: 10.1126/scisignal.2004145

This PDF file includes:

Other Supplementary Material for this manuscript includes the following:
(available at www.sciencesignaling.org/cgi/content/full/6/289/ra70/DC1)

Table S5 (Microsoft Excel format). *D. melanogaster* dsRNAi screen.
Table S6 (Microsoft Excel format). Molecular complex analysis (*D. melanogaster*).
Table S7 (Microsoft Excel format). Evolutionarily conserved complexes between *D. melanogaster* and *S. cerevisiae*.
Table S8 (Microsoft Excel format). *S. cerevisiae* strains.
Table S9 (Microsoft Excel format). Primers.
Raw image files S1 to S4.

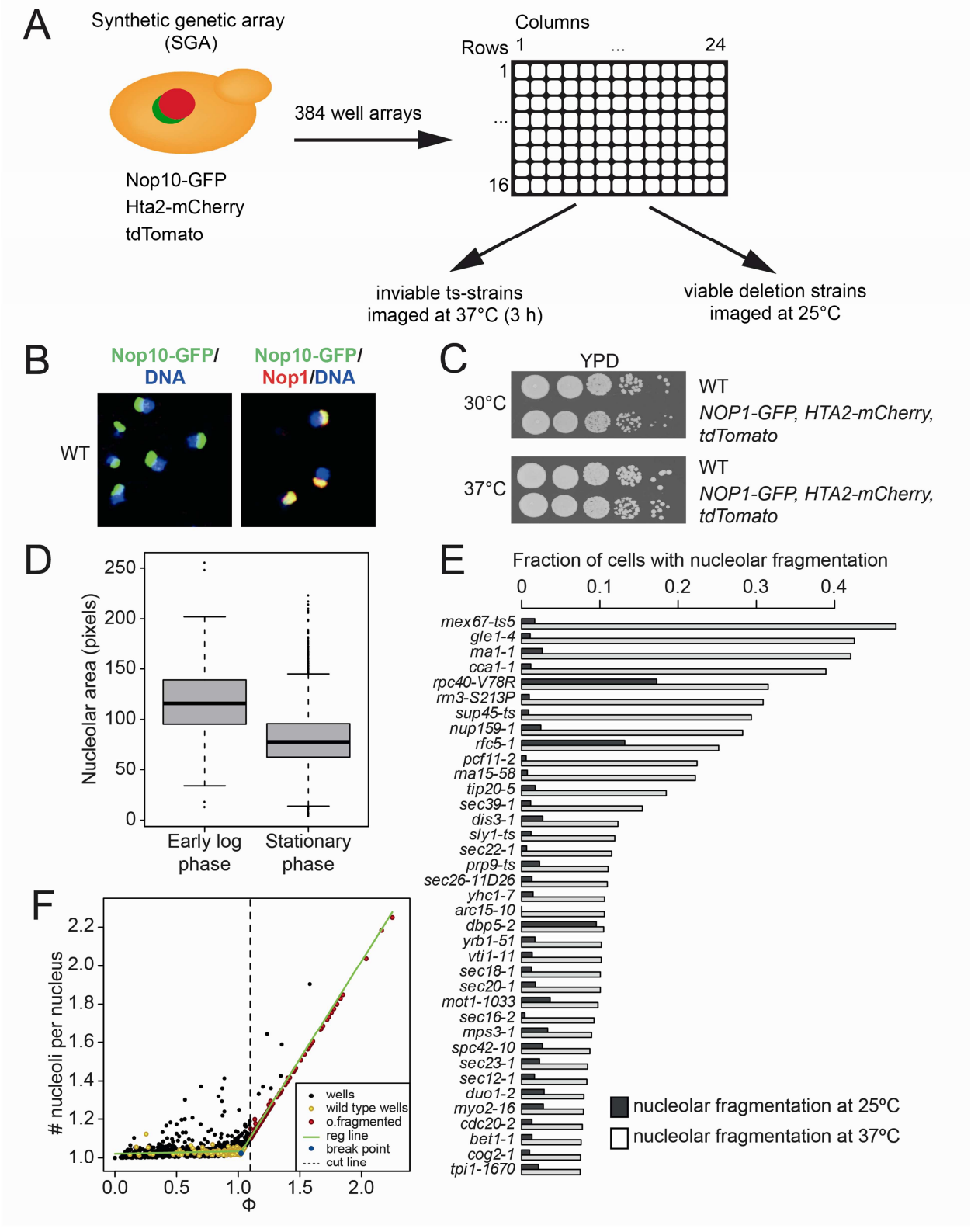
A
Synthetic genetic array (SGA)
Nop10-GFP
Hta2-mCherry
tdTomato
384 well arrays
Columns
Rows 1 ... 24
1
...
16
inviable ts-strains imaged at 37°C (3 h)
viable deletion strains imaged at 25°C
B
Nop10-GFP/ DNA
Nop10-GFP/ Nop1/DNA
WT
C
YPD
30°C
WT
NOP1-GFP, HTA2-mCherry, tdTomato
37°C
WT
NOP1-GFP, HTA2-mCherry, tdTomato
D
Nucleolar area (pixels)
250
200
150
100
50
0
Early log phase
Stationary phase
E
Fraction of cells with nucleolar fragmentation
0
0.1
0.2
0.3
0.4
mex67-ts5
gle1-4
rna1-1
cca1-1
rpc40-V78R
rrn3-S213P
sup45-ts
nup159-1
rfc5-1
pcf11-2
rna15-58
tip20-5
sec39-1
dis3-1
sly1-ts
sec22-1
prp9-ts
sec26-11D26
yhc1-7
arc15-10
dbp5-2
yrb1-51
vti1-11
sec18-1
sec20-1
mot1-1033
sec16-2
mps3-1
spc42-10
sec23-1
sec12-1
duo1-2
myo2-16
cdc20-2
bet1-1
cog2-1
tpi1-1670
nucleolar fragmentation at 25ºC
nucleolar fragmentation at 37ºC
F
nucleoli per nucleus
2.2
2.0
1.8
1.6
1.4
1.2
1.0
0.0
0.5
1.0
1.5
2.0
Φ
wells
wild type wells
o.fragmented
reg line
break point
cut line

Figure S1. SGA screen for nucleolar defects in *S. cerevisiae.*

(**A**) Schematic overview of the SGA screen.

(**B**) Co-localization of Nop10-GFP and Nop1 (antibody staining) in *S. cerevisiae*. Images are representative of at least 5 independent biological replicates.

(**C**) Growth of the SGA query strain compared to wild-type at 30℃ and 37℃. Images are representative of 3 independent biological replicates.

(**D**) Box plot illustrating the decrease of nucleolar size in stationary phase yeast cells compared to cells in log phase.

(**E**) Bar plot representing 38 nucleolar fragmentation phenotypes of the essential gene collection imaged and quantified at the permissive and non-permissive temperature. Values on the y-axis represent the fraction of nuclei with fragmented nucleoli in a well (for full list of identified nucleolar fragmentation phenotypes see Table S1).

(**F**) Average number of nucleoli plotted as a function of fragmentation index. Control wells are shown as yellow circles, while the rest of the wells are colored in grey. The green line represents piece-wise linear regression model fitted to the data, where a blue dot corresponds to a break point. The value of the fragmentation index corresponding to a threshold marking over-fragmented nucleoli is shown as a dashed line. Red circles depict wells containing over-fragmented nucleoli.

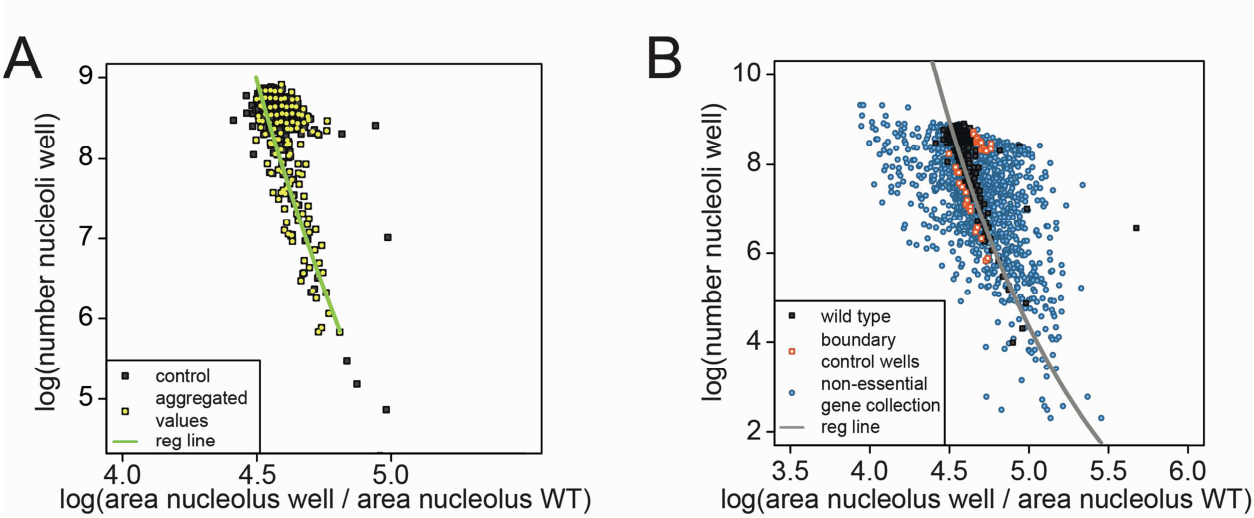

Figure S2. Supporting graphs for nucleolar size quantification.

(**A**) Regression analysis for nucleolar area and number of cells in the well for the essential collection. Non-linear regression model (green line) fitted to the aggregated wild-type data. The control wells are shown as grey squares. The aggregated values used to construct the regression model are represented as yellow circles.

(**B**) The regression model fitted to the whole essential collection. The regression line is shown in grey. The grey squares mark WT control wells, whereas the rest of the wells in the collection are plotted as blue circles. The white squares correspond to the boundary control wells used to discriminate between wells containing over- or under-sized nucleoli and wild-type controls.

A

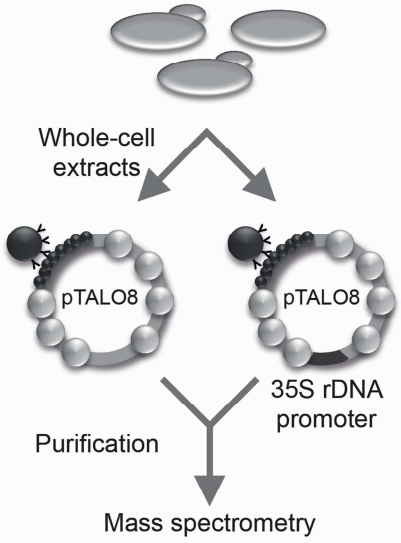

B

Sub-complex	Protein hits (**bold**)
upstream activating factor (UAF)	**Rrn5**, **Rrn9**, **Rrn10**, **Uaf30**
core factor (CF)	Rrn6, Rrn7, Rrn11
regulator of nucleolar silencing and telophase exit (RENT) complex	**Net1**, **Cdc14**, Sir2
TATA-binding protein (TBP)	**Spt15**
other	Rrn3, **Reb1**
FACT complex *	**Spt16, Pob3**
HIR complex *	**Hir2**
RSC complex *	**Rsc1, Rsc2, Rsc3, Rsc4, Rsc6, Rsc7, Rsc8, Sth1, Sfh1**

C

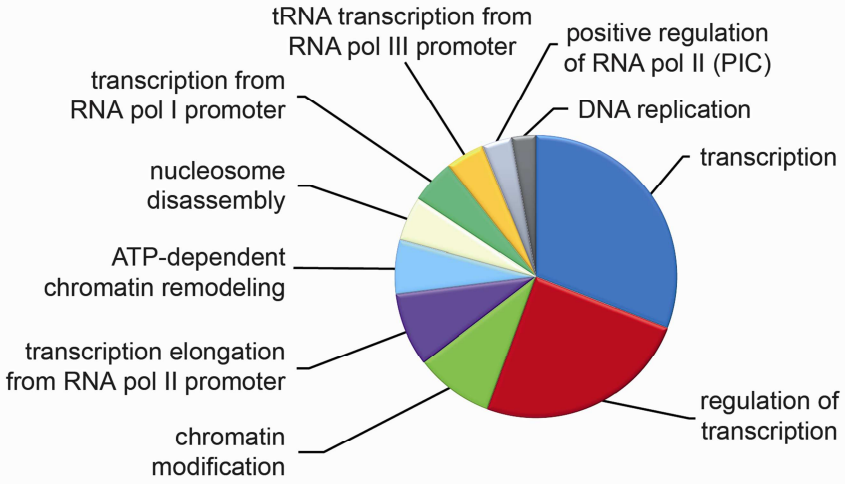

D

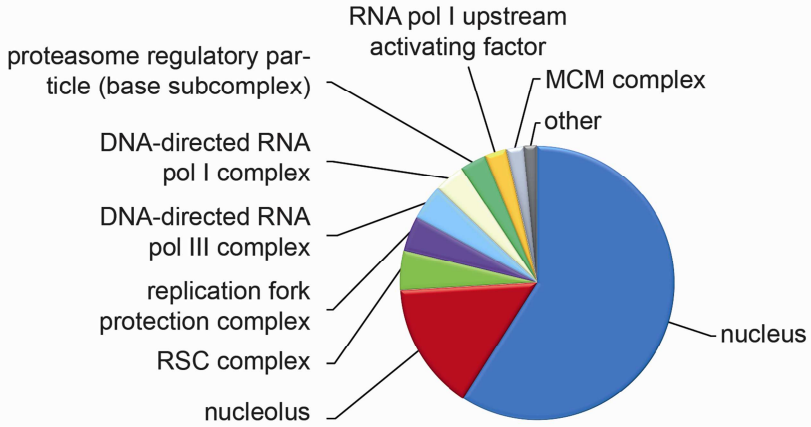

Figure S3. The rDNA promoter proteome.

(**A**) Schematic overview of the affinity purification of TALO8-minichromosomes. Minichromosomes containing the 35S rDNA promoter region and LacO repeats are captured by Flag-LacI affinity purification.

(**B**) Table of previously identified and unidentified (asterisks) Pol I transcriptional regulators. Hits found in the TALO8-rDNA purification are highlighted bold.

(**C**) Functional GO term analysis of the identified 35S rRNA promoter-associated proteome upon TALO8 purification.

(**D**) Localization GO term analysis of the identified 35S rRNA promoter-associated proteome upon TALO8 purification.

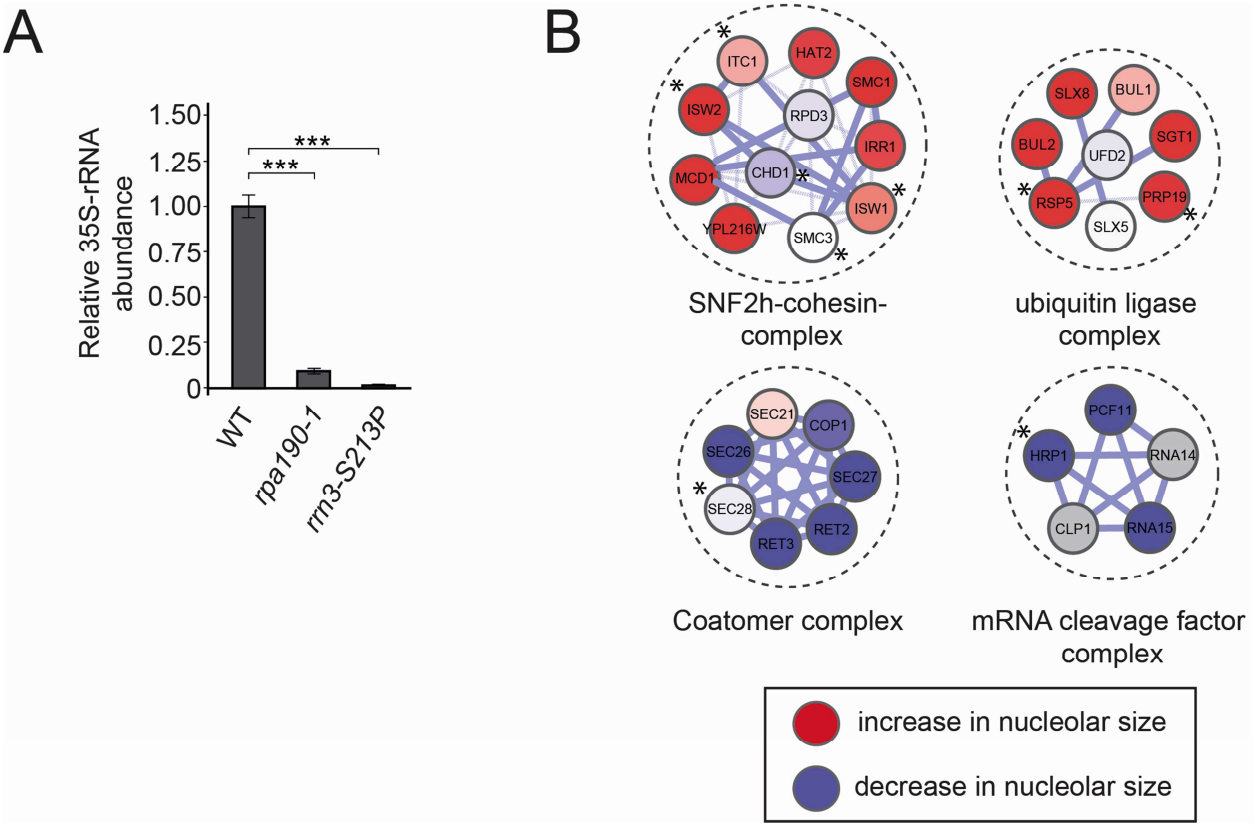

Figure S4. Examples of protein complexes that scored in the SGA screen.

(**A**) Validation of the qRT-PCR strategy to quantify differences in 35S rRNA abundance. Bars represent the means ± SD of 5 independent biological replicates. ****P*<0.001.

(**B**) Examples of molecular complexes not implicated in transcriptional regulation identified in the SGA screen (red: increase in nucleolar size, blue: decrease in nucleolar size, grey: genes which have not been screened, asterisks denote proteins identified in the TALO8 purification).

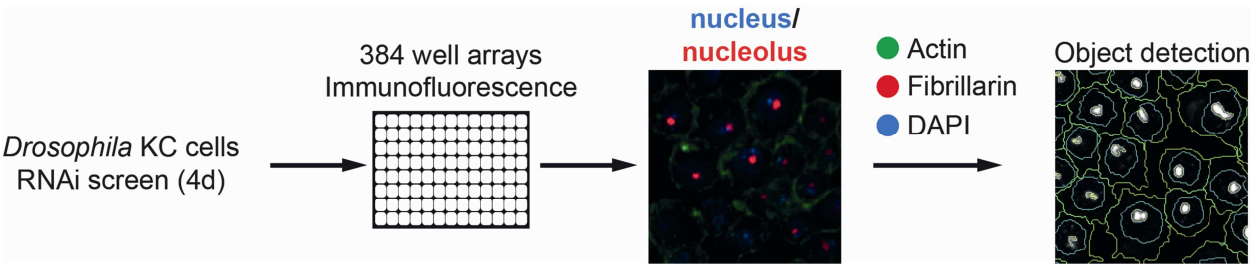

Figure S5. A genome-wide RNAi screen for nucleolar size defects in *Drosophila* cell culture. Schematic overview of the RNAi screening strategy (Note: right panel shows a close up of the computer-based segregation of objects of the stained KC cells).

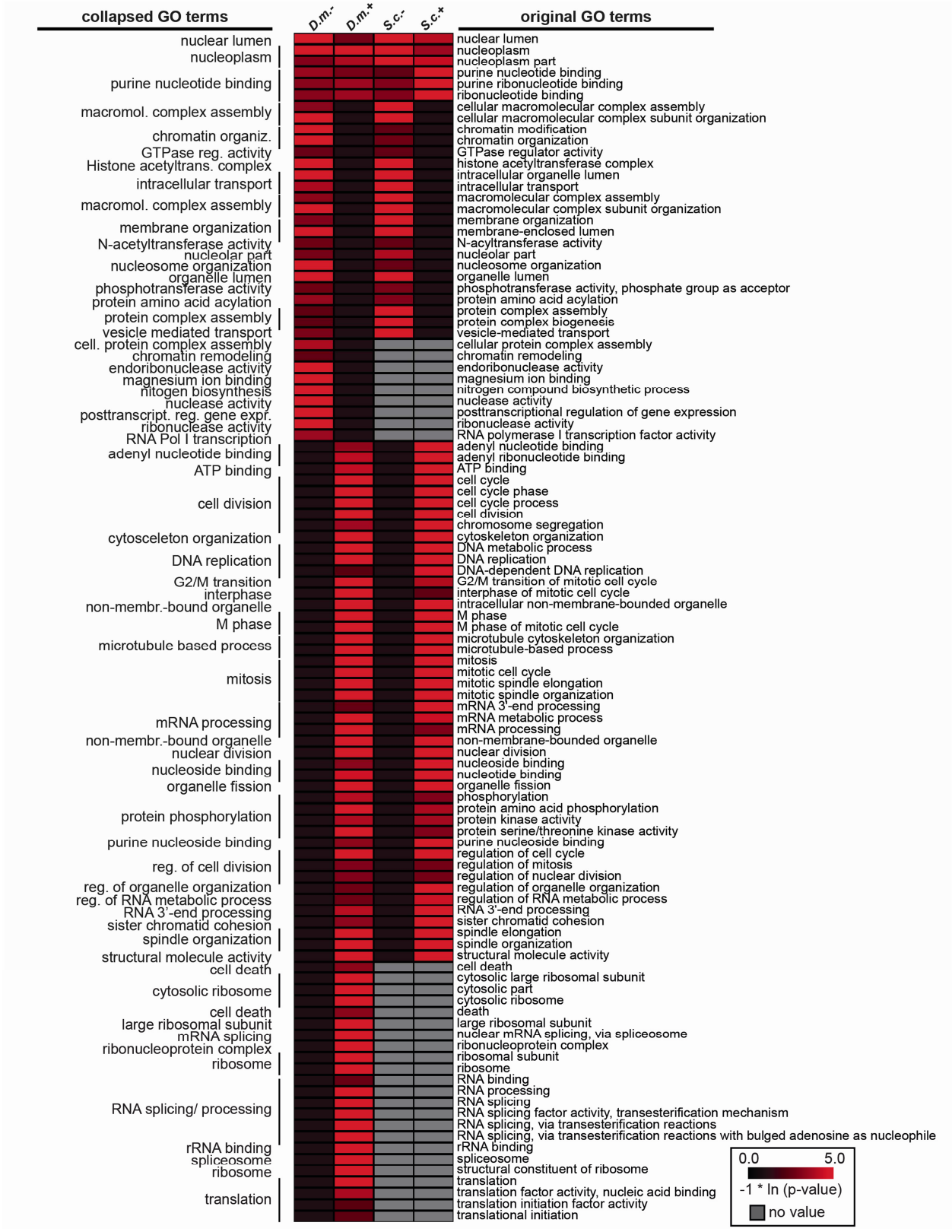
collapsed GO terms
original GO terms
D.m.-
D.m.+
S.c.-
S.c.+
nuclear lumen
nucleoplasm
nucleoplasm part
purine nucleotide binding
purine ribonucleotide binding
ribonucleotide binding
cellular macromolecular complex assembly
cellular macromolecular complex subunit organization
chromatin modification
chromatin organization
GTPase regulator activity
histone acetyltransferase complex
intracellular organelle lumen
intracellular transport
macromolecular complex assembly
macromolecular complex subunit organization
membrane organization
membrane-enclosed lumen
N-acyltransferase activity
nucleolar part
nucleosome organization
organelle lumen
phosphotransferase activity, phosphate group as acceptor
protein amino acid acylation
protein complex assembly
protein complex biogenesis
vesicle-mediated transport
cellular protein complex assembly
chromatin remodeling
endoribonuclease activity
magnesium ion binding
nitrogen compound biosynthetic process
nuclease activity
posttranscriptional regulation of gene expression
ribonuclease activity
RNA polymerase I transcription factor activity
adenyl nucleotide binding
adenyl ribonucleotide binding
ATP binding
cell cycle
cell cycle phase
cell cycle process
cell division
chromosome segregation
cytoskeleton organization
DNA metabolic process
DNA replication
DNA-dependent DNA replication
G2/M transition of mitotic cell cycle
interphase of mitotic cell cycle
intracellular non-membrane-bounded organelle
M phase
M phase of mitotic cell cycle
microtubule cytoskeleton organization
microtubule-based process
mitosis
mitotic cell cycle
mitotic spindle elongation
mitotic spindle organization
mRNA 3'-end processing
mRNA metabolic process
mRNA processing
non-membrane-bounded organelle
nuclear division
nucleoside binding
nucleotide binding
organelle fission
phosphorylation
protein amino acid phosphorylation
protein kinase activity
protein serine/threonine kinase activity
purine nucleoside binding
regulation of cell cycle
regulation of mitosis
regulation of nuclear division
regulation of organelle organization
regulation of RNA metabolic process
RNA 3'-end processing
sister chromatid cohesion
spindle elongation
spindle organization
structural molecule activity
cell death
cytosolic large ribosomal subunit
cytosolic part
cytosolic ribosome
death
large ribosomal subunit
nuclear mRNA splicing, via spliceosome
ribonucleoprotein complex
ribosomal subunit
ribosome
RNA binding
RNA processing
RNA splicing
RNA splicing factor activity, transesterification mechanism
RNA splicing, via transesterification reactions
RNA splicing, via transesterification reactions with bulged adenosine as nucleophile
rRNA binding
spliceosome
structural constituent of ribosome
translation
translation factor activity, nucleic acid binding
translation initiation factor activity
translational initiation
nuclear lumen
nucleoplasm
purine nucleotide binding
macromol. complex assembly
chromatin organiz.
GTPase reg. activity
Histone acetyltrans. complex
intracellular transport
macromol. complex assembly
membrane organization
N-acetyltransferase activity
nucleolar part
nucleosome organization
organelle lumen
phosphotransferase activity
protein amino acid acylation
protein complex assembly
vesicle mediated transport
cell. protein complex assembly
chromatin remodeling
endoribonuclease activity
magnesium ion binding
nitrogen biosynthesis
nuclease activity
posttranscript. reg. gene expr.
ribonuclease activity
RNA Pol I transcription
adenyl nucleotide binding
ATP binding
cell division
cytosceleton organization
DNA replication
G2/M transition
interphase
non-membr.-bound organelle
M phase
microtubule based process
mitosis
mRNA processing
non-membr.-bound organelle
nuclear division
nucleoside binding
organelle fission
protein phosphorylation
purine nucleoside binding
reg. of cell division
reg. of organelle organization
reg. of RNA metabolic process
RNA 3'-end processing
sister chromatid cohesion
spindle organization
structural molecule activity
cell death
cytosolic ribosome
cell death
large ribosomal subunit
mRNA splicing
ribonucleoprotein complex
ribosome
RNA splicing/ processing
rRNA binding
spliceosome
ribosome
translation
0.0
5.0
-1 * ln (p-value)
no value

Figure S6. Comparative GO term analysis between the *S. cerevisiae* SGA and the *D. melanogaster* RNAi screens.

Heatmap displaying the natural log transformed p-values for the respective GO terms (*D.m.*: *D. melanogaster, S.c.*: *S. cerevisiae,* decrease (-) or increase (+) in nucleolar size).

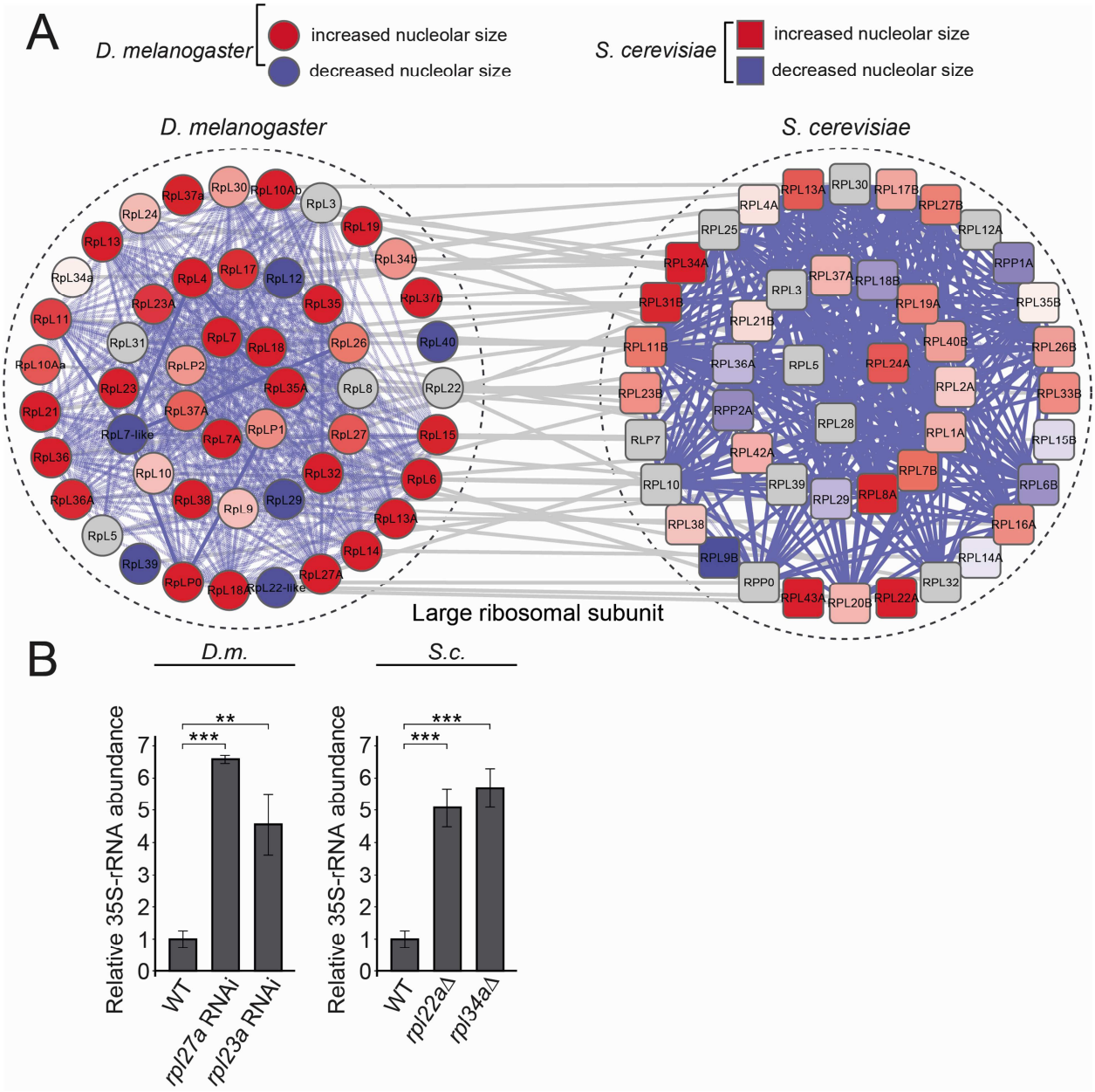

Figure S7. Altered nucleolar size upon loss of ribosomal function in *D. melanogaster* and *S. cerevisiae*.

(**A**) Complex map of the large ribosomal subunit in *D. melanogaster* (round nodes) and *S. cerevisiae* (rectangular nodes) with the respective nucleolar size phenotypes color coded (red: increase in nucleolar size, blue: decrease in nucleolar size, grey: genes which have not been screened or for which no homolog exists in the respective species, blue lines denote protein-protein interaction data, grey lines connect homologous genes).

(**B**) Increase of 35S rRNA abundance upon loss of ribosomal subunits in *D. melanogaster* and *S. cerevisiae* measured by qRT-PCR. Bars represent the means ± SD of 5 independent biological replicates. ****P*<0.001; ***P*<0.01

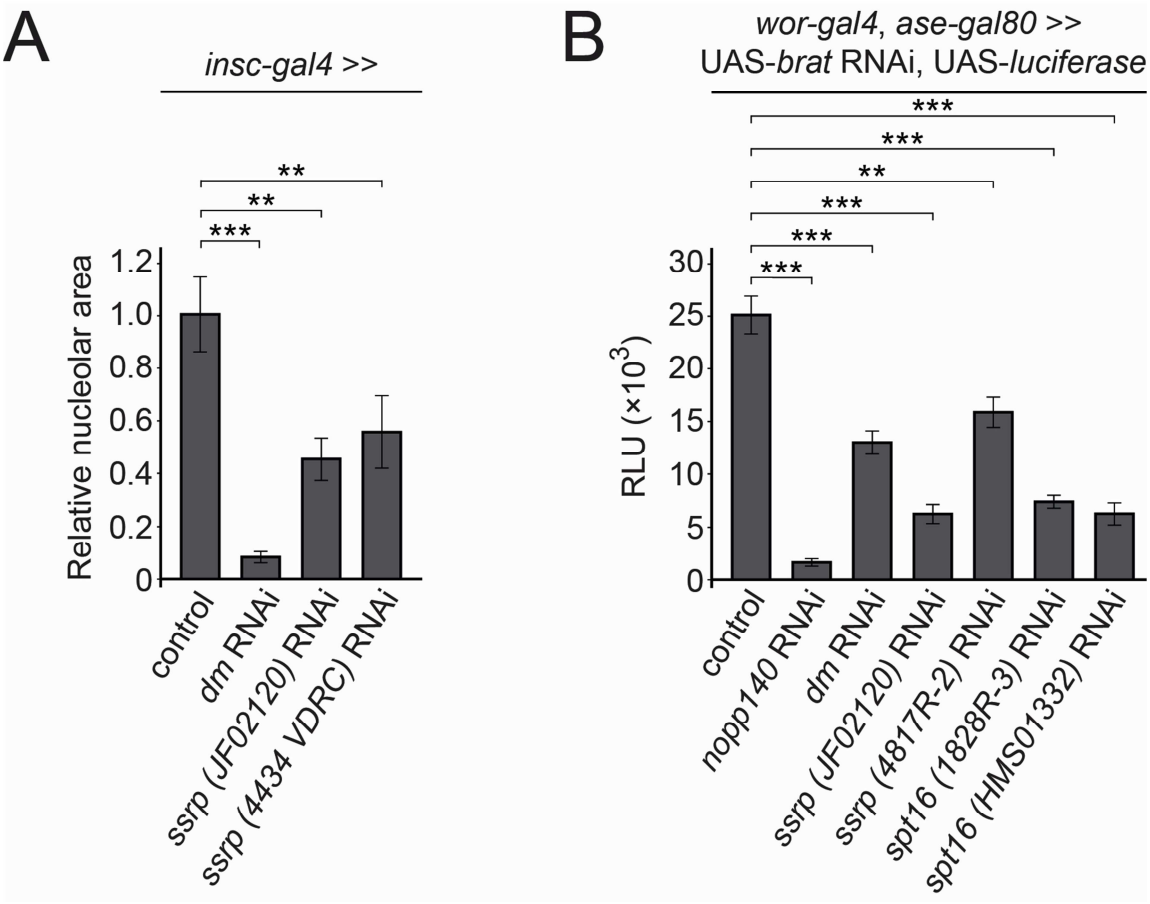

Figure S8. The *Drosophila* FACT complex is required for cell growth.

(**A**) Complete data set of the experiment shown in Fig. 5C assaying nucleolar size upon *ssrp* RNAi using two independent non-overlapping RNAi constructs. Bars represent the means ± SD of 5 or more independent biological replicates. ****P*<0.001; ***P*<0.01

(**B**) Complete data set of the experiment shown in Fig. 5E quantifying tumor growth based on luciferase expression using independent, non-overlapping RNAi lines targeting *nopp140*, *dm*, *ssrp* and *spt16*. Bars represent the means ± SD of 4 independent biological replicates. ****P*<0.001; ***P*<0.01

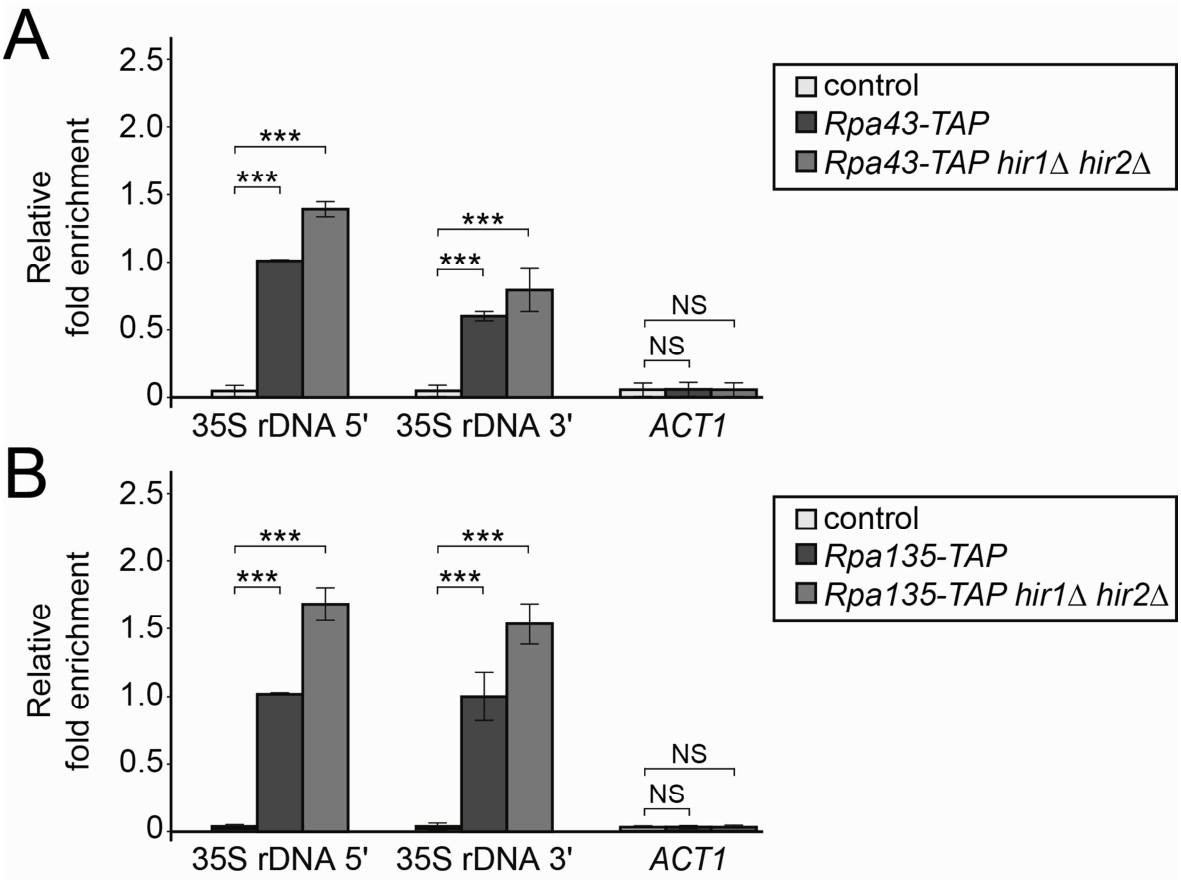

Figure S9. The HIR complex double-mutant *hir1*Δ*hir2*Δ shows increased Pol I occupancy over the 35S rDNA region.

ChIP qPCR analysis of TAP-tagged Pol I subunits Rpa43 (**A**) and Rpa135 (**B**) at the 35S rDNA region and the *ACT1* control region was performed. Values are normalized relative to a non-transcribed region (NTR) and the fold enrichment of wild-type from the 5' region of the rDNA locus was set to 1. Bars represent the means ± SD of 3 independent biological replicates. ****P*<0.001; NS, not significant

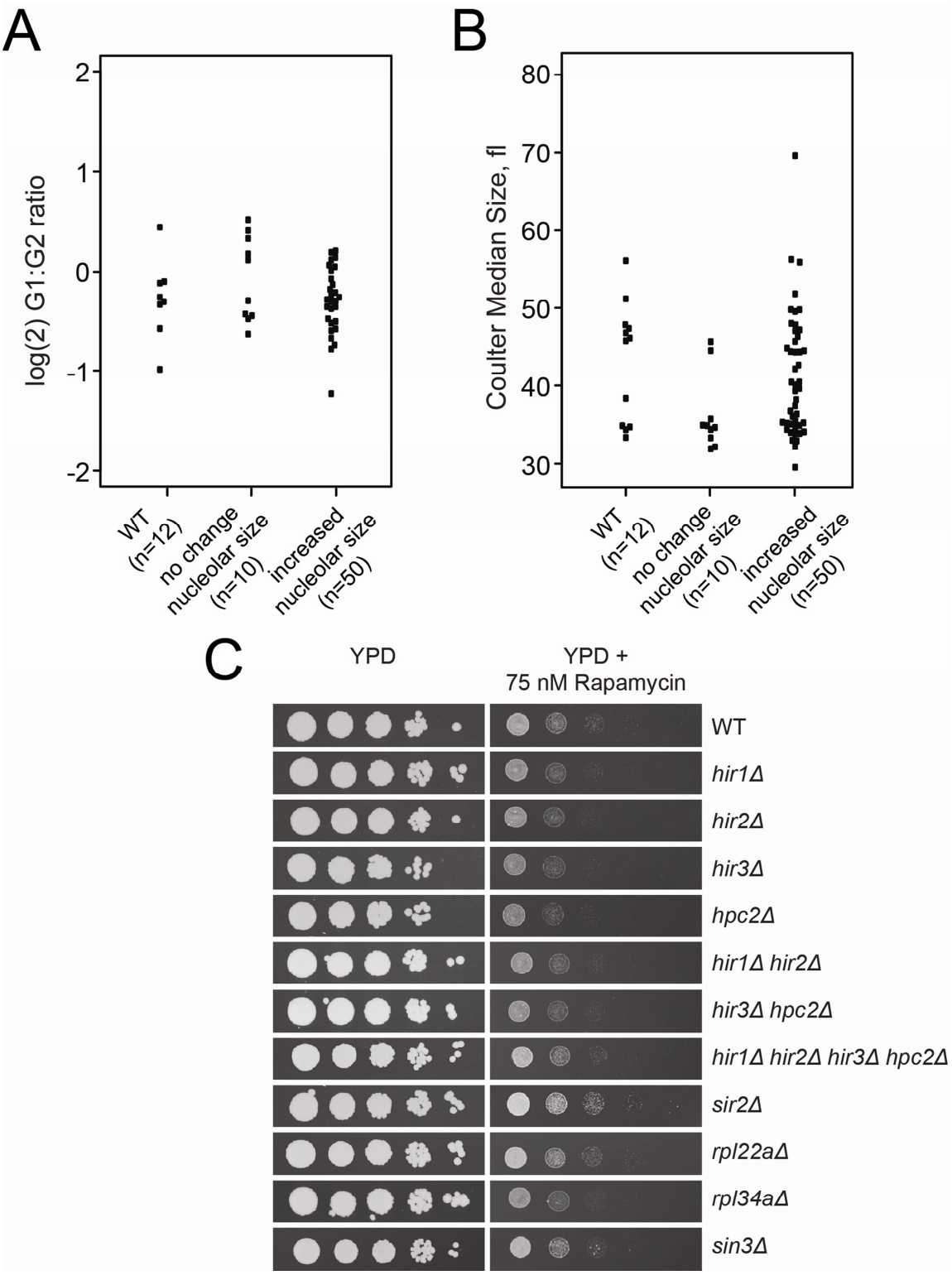
A
log(2) G1:G2 ratio
2
1
0
-1
-2
WT (n=12)
no change nucleolar size (n=10)
increased nucleolar size (n=50)
B
Coulter Median Size, fl
80
70
60
50
40
30
WT (n=12)
no change nucleolar size (n=10)
increased nucleolar size (n=50)
C
YPD
YPD + 75 nM Rapamycin
WT
hir1Δ
hir2Δ
hir3Δ
hpc2Δ
hir1Δ hir2Δ
hir3Δ hpc2Δ
hir1Δ hir2Δ hir3Δ hpc2Δ
sir2Δ
rpl22aΔ
rpl34aΔ
sin3Δ

Figure S10. Growth measurements of HIR complex mutants.

(**A**) Cell cycle distribution determined by flow cytometry. N=10 or more independent biological replicates.

(**B**) Cell size distribution in mid-log phase. N=10 or more independent biological replicates.

(**D**) Colony growth experiment in the presence and absence of rapamycin. Tenfold serial dilutions of the indicated yeast strains were spotted on YPD plates with or without rapamycin (75 nM) and imaged after incubation for two days at 30℃. In contrast to the transcription silencing mutant *sir3*Δ, used as positive control, HIR complex mutants do not show increased growth in the presence of rapamycin in comparison to wild-type. Images are representative of 3 independent biological replicates.